

In-orbit performance of the Ozone Monitoring Instrument

Johan de Vries*^a, Robert Voors^b, Ruud Dirksen^{b/c},
Marcel Dobber^b

^a Dutch Space BV, Newtonweg 1, 2333 CP Leiden, The Netherlands

^bRoyal Netherlands Meteorological Institute (KNMI), Wilhelminalaan 10, 3732 GK De Bilt, The Netherlands

^cSpace Research Organization Netherlands (SRON), Sorbonnelaan 2, 3584 CA Utrecht, The Netherlands¹

ABSTRACT

In July 2004 Nasa's AURA satellite was launched carrying the Dutch-Finnish Ozone Monitoring Instrument and since then it is producing high quality trace gas measurements of a.o. ozone and NO₂. The OMI is a non-scanning nadir viewing spectrograph with a wavelength coverage of 270 to 500 nm and a spectral resolution of 0.4 to 0.7 nm. It has a large spatial field-of-view of 114 degrees perpendicular to the flight direction and uses the resulting swath of 2600 km to measure the complete globe in a single day with ground pixels of nominally 13 km x 24 km. After a brief instrument overview, this paper discusses a number of in-flight performance issues, such as the wavelength calibration and the stray light correction

OMI's wavelength calibration is based on fitting the sun's Fraunhofer structures, both on sun irradiance spectra and Earth radiance spectra. For the latter the cloud structures impact the wavelength results via inhomogeneous illumination of the spectrometer slit. This is explained together with the basics of a correction algorithm.

OMI has a carousel with three on-board sun diffusers. Measurements with the quartz volume diffuser will be used to show remaining diffuser features in the data. The measured irradiances are compared to the results obtained by convolving the high-resolution solar reference spectrum with the accurately calibrated spectral slit functions.

In the in-flight measurement data in the wavelength range below 300 nm spatial stray light features are observed, resulting from clouds observed at wavelengths above 300 nm. These features are shown together with an explanation of the means to analyze the in-orbit stray light performance.

Keywords: UV-Visible spectrograph, trace gas monitoring, calibration.

1. INTRODUCTION

The primary objective of the OMI on AURA is to obtain global measurements of a number of trace gases in both the troposphere and stratosphere. These measurements are meant to address science questions on the recovery of the ozone layer, the depletion of ozone at the poles, tropospheric pollution and climate change.

OMI delivers spectral radiances and irradiances in the UV-Visible wavelength range and these are used to retrieve the following primary data products: ozone total column, ozone vertical profile, UV-B flux, NO₂ total column, aerosol optical thickness, effective cloud cover and cloud top pressure. Next to these there are total column products for the following additional gases: SO₂, BrO, HCHO and OCIO.

The total column and the profile are retrieved from nadir observations of backscattered sun light from the Earth's atmosphere in the wavelength range of 270 to 500 nm. Within this range, the spectral properties are such that it is possible to use both DOAS and TOMS-type of algorithms² for column retrievals of the various atmospheric constituents. These are similar to those of instruments like GOME, SCIAMACHY, TOMS and SBUV.

¹ *j.de.vries@dutchspace.nl; phone +31 5245879; fax +31 5245835; P.O. box 32070, 2303 DB Leiden, the Netherlands

The ozone vertical profile is obtained from the rapid increase of the absorption cross-section towards shorter wavelengths in the UV. The cloud top pressure is retrieved from both the O₂-O₂ complex at 477 nm and from the Ring effect due to inelastic Raman scattering at 390 - 400 nm. The cloud cover and aerosol optical thickness are obtained from the broader wavelength dependency of the backscattered sunlight.

OMI has a fairly high spatial resolution combined with coverage of the complete globe each day. This spatial resolution (nominally 13 x 24 km² and in zoom-in mode 13 x 12 km²) has firstly been implemented to have a good probability for observing cloud-free ground pixels, and to have a maximum of data with sensitivity down to surface level. It also helps to actually study local effects, such as industrial pollution, volcanic eruptions, lightning effects and biomass burning. Data on tropospheric pollution is essential for studying human impact on the Earth's atmosphere and climate.

OMI was launched in July 2004 on NASA's AURA satellite. The instrument has been developed by Dutch and Finnish industry in close collaboration with the climate research and meteorological community and under contract with the Netherlands Agency for Aerospace Programmes (NIVR) and the Finnish Meteorological Institute (FMI). The Royal Dutch Meteorological Institute (KNMI) is the PI institute for the OMI instrument and leads the international OMI Science Team of approximately 60 members.



Figure 1 Launch of the Nasa's AURA satellite with the Ozone Monitoring Instrument on July 15, 2004

2. OMI SYSTEM DESCRIPTION

The OMI System consists of the OMI instrument hardware and the OMI ground segment. The function of the ground segment is both to perform instrument operations and the science data processing using the OMI 0-1b processor. This processor converts Level 0 instrument data into Level 1b science data. The instrument hardware is discussed in this section and there are some words on the 0-1b processor.

The OMI instrument is a compact nadir viewing imaging spectrograph with two channels each having a two-dimensional frame transfer CCD. In one dimension the spectrum is registered and in the other the large (114°) field-of-view perpendicular to the flight direction. This swath is wide enough to have daily global coverage with only small gaps at the equator and increasing orbit overlaps at higher latitudes.

Figure 2 shows the conceptual design of the instrument with the large swath out of the plane of the paper. The telescope part of OMI consists of a primary mirror, a polarization scrambler and a secondary mirror that focuses the incident radiances on the spectrograph slit. Sun light enter the instrument through a solar port and illuminate a reflection diffuser. A folding mirror couples the diffuser signal into main optical path just before the polarization scrambler. An on-board White Light Source (WLS) can be coupled in through a transmission diffuser and the same folding mirror. For on-ground calibration purposes this optical path was also used by mounting external stimuli on a calibration port close to the WLS. After the slit, in the spectrograph, the beam is split, using a dichroic, into two channels: the UV (270 - 380 nm)

and the Visible (350 - 500 nm). The UV channel is optically separated into two sub-channels: UV-1 (270 - 314 nm) and UV-2 (306 - 380 nm). This reduces the stray light at smaller wavelengths. Furthermore, the UV-1 sub-channel is scaled down by a factor two, meaning that both the spectral and spatial sampling distances are larger by a factor two as compared to the UV-2 and Visible. This is to improve the ratio between useful and dark signals in the UV1. The channel overlaps are made fairly smooth by avoiding the use of dichroic designs with high gradients. This is beneficial for the instrument stability.

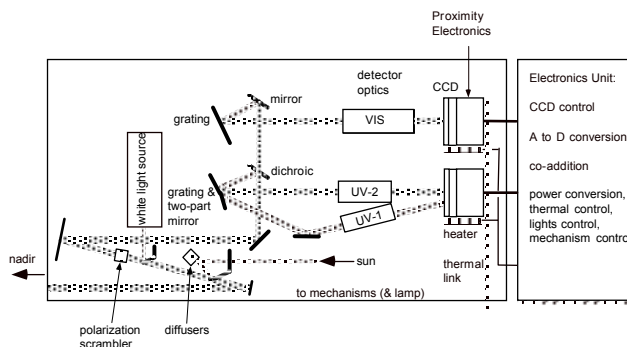


Figure 2 Conceptual design of the OMI-EOS.

The spectral sampling distances are 0.32 nm, 0.15 nm and 0.21 nm for UV-1, UV-2 and VIS, respectively. The ratio between resolution and sampling distance is about 3 to avoid any difficulties caused by aliasing in the process of trace gas retrieval. It was checked by simulation that with these design parameters trace gas retrieval can indeed be performed with the required accuracy².

The spatial sampling distance and resolution in the flight direction are determined by the detector exposure times and the width of the spectrometer slit. The basic detector exposure time is 0.4 s corresponding to a distance on ground of about 3 km. The spectrometer slit width is such that the spatial resolution in the flight direction is about 10 km. The spatial sampling distance and resolution in the swath direction are determined by the CCD pixel size and the optical focusing quality. This sampling is also about 3 km (in UV-2 and VIS) and the corresponding resolution is about the same.

The CCD detector has a frame transfer layout to allow simultaneous exposure and readout of the previous exposure. This allows for fair pixel readout rates (133 kHz) and avoids data loss during detector readout.

Data from several basic ground pixels are added to come to the minimum available ground pixel size of about 12 x 13 km at nadir. During each read-out of the CCD several pixel rows are binned, so spectra from neighboring viewing directions are summed. Also, subsequent exposures are digitally co-added. In this way the readout noise is minimized, the signal-to-noise is increased and the internal data rate decreased. For each CCD it is possible to select a wavelength (pixel column) for which the co-addition is skipped. This is implemented to have for each detector for one wavelength data at the smallest sampling distance on clouds or albedo.

The in-flight calibration is maintained as follows:

- Absolute radiometric calibration is taken care of by weekly measurement of the Sun via a grinded aluminium reflection diffuser. The instrument is equipped with a second aluminium reflection diffuser, which is measured once per month. The two aluminium diffusers are expected to have the same degradation as a function of the integrated sun light exposure time. By using different observation frequencies the relative degradation can be monitored. A third diffuser is a volume reflection diffuser that was implemented to minimise the impact of wavelength- and viewing angle-dependent interference effects from the diffuser surface. Because of its smooth surface the volume diffuser only introduces spectral structures with at least ten times smaller amplitude than observed for the aluminium diffusers. The volume diffuser is measured once per day. The diffuser beams illuminate the complete slit such that the reference spectra are available for all viewing directions within the field-of-view. The diffusers are well protected from contamination while not in use.
- Relative radiometric calibration is performed using a White Light Source (WLS). Two green LEDs per spectral (sub-) channel are used to monitor the CCD detector performance. The two LEDs fairly uniformly illuminate the CCDs, also in the case one of the two fails.

- Spectral calibration is being performed using Fraunhofer features in solar and nadir spectra. The slit function of OMI has been accurately calibrated on pixel level during the on-ground calibration. This slit function permits to establish a wavelength calibration between a high-resolution solar spectrum and the observed features.
- Dark signal calibration is performed at the dark side of the orbit using dark measurements with the same clock settings as used for the Earth measurements. In addition, long dark measurements with exposure times of up to 136 seconds are performed. The clock sequencer electronics allows having both dark current images for the image and the readout sections of the CCD and every image is preceded with readout of the register to have electronics offset data. Each image contains also dark current information from masked pixels on the CCD.
- Stray light and exposure smear signal are monitored by dedicated pixels at the sides of the images.

The OMI 0-1b processor has algorithms to invert each of the instrument artifacts or properties and it sets flags for user notification whenever limits are passed. There are algorithms in the following classes.

- Detector pixel related flagging algorithms, i.e. Dead pixels, Random telegraph pixels, Saturated pixels, Transient pixels
- Simple algorithms without accuracy impact, i.e. Co-addition division, ADC conversion, Electronic conversion, Binning factor division, Exposure time division, Calculation of measurement noise
- Detector and electronics artifact related, i.e. Offset correction, Non-linearity correction, Dark current correction, Exposure smear correction, Relative pixel-to-pixel sensitivity correction (PRNU)
- (Ir-) Radiance correction algorithms, i.e. Stray light correction, Slit irregularity correction, Radiance and irradiance sensitivity correction, Irradiance elevation angle averaging, to reduce the effect from diffuser features
- Spectral calibration based on Fraunhofer line fitting and wavelength assignment, together with Doppler shift corrections
- Geolocation

This paper discusses the, wavelength fitting and assignment and checks the measured sun spectra and the stray light performance and correction.

3. Wavelength Calibration

3.1 Introduction

From previous hyper-spectral satellite instruments, most notably the Global Ozone Monitoring Experiment (GOME), it was shown that in order to accurately calibrate the wavelength scale of the spectra, it is not necessary to carry a reference line lamp onboard. The absorption lines in the solar spectrum itself provide more than enough information for a very accurate wavelength calibration. Therefore it was decided not to include a line lamp in the design of OMI.

For this approach to work, one needs a solar reference spectrum with a very accurate wavelength scale, to which the measurements can be fitted. For solar measurements it is no surprise this approach works well. For Earth reflected measurements the solar signal is modified by the very constituents like O₃ and NO₂ that we wish to study with OMI. Also the Ring effect⁵ influences the appearance of the reflected spectrum and therefore the wavelength calibration. When calibrating the wavelength scale of 'Earth' measurements this is taken into account.

The wavelength scale in the L1B products is reported as polynomial coefficients (4th order) instead of wavelength per pixel. The reported scale is not based on a wavelength calibration per spectrum, on the one hand because of the high computational cost of the wavelength calibration algorithm, on the other because of the excellent thermal stability of OMI. It was argued that temperature changes in the optics would account for most of the change in wavelength scale. And since the temperature changes are very small and very smooth over time, this can in principle be used to derive more accurate wavelength scales than can be achieved by inspecting individual spectra. So, when OMI was launched the wavelength scale was calculated based on a reference wavelength scale and the temperature of the optical bench, which is accurately measured for each measurement.

3.2 The Sting

When the first OMI measurements came in, it became clear that individual results of the in-orbit wavelength calibration showed much stronger variability than was expected based on the observed temperature changes. This variability is real and not due to a problem with the wavelength calibration method. Furthermore, it was shown that this observed variability in the wavelength scale correlates with the variability of the radiance level during a single 2 second observation. In standard operations, such a single radiance measurement comprises 5 co-added measurements of 0.4 seconds. For most wavelengths, the information of these 5 individual measurements is not recorded. However, for a single wavelength, this information is retained in the so-called small pixel radiance and can be used to determine the variability during a 2second period. As a result of the high degree of correlation between the variability in the small pixel signal and the change in wavelength between two measurements, the wavelengths as assigned in the LIB product can be ‘corrected’.

3.3 The physical mechanism and correction

So, the rate of change of the radiance level correlates with the observed change in the wavelength scale. This behaviour can be understood by considering the optics of OMI. Basically, light enters the instrument via an entrance slit, is reflected off a grating and is then imaged on the CCD. When the entrance slit is not homogeneously illuminated, this effectively causes a change in the shape of the instrument transfer function or ‘slit function’. A symmetric slit function that becomes asymmetric because of the inhomogeneous illumination of the entrance slit causes a shift in the wavelength scale. This mechanism also explains why the observed wavelength shifts are largest in the VIS channel, where the relative influence on the radiance level caused by scattered clouds is largest. As expected, the UV1 channel (wavelength < 310 nm) is hardly influenced by this effect.

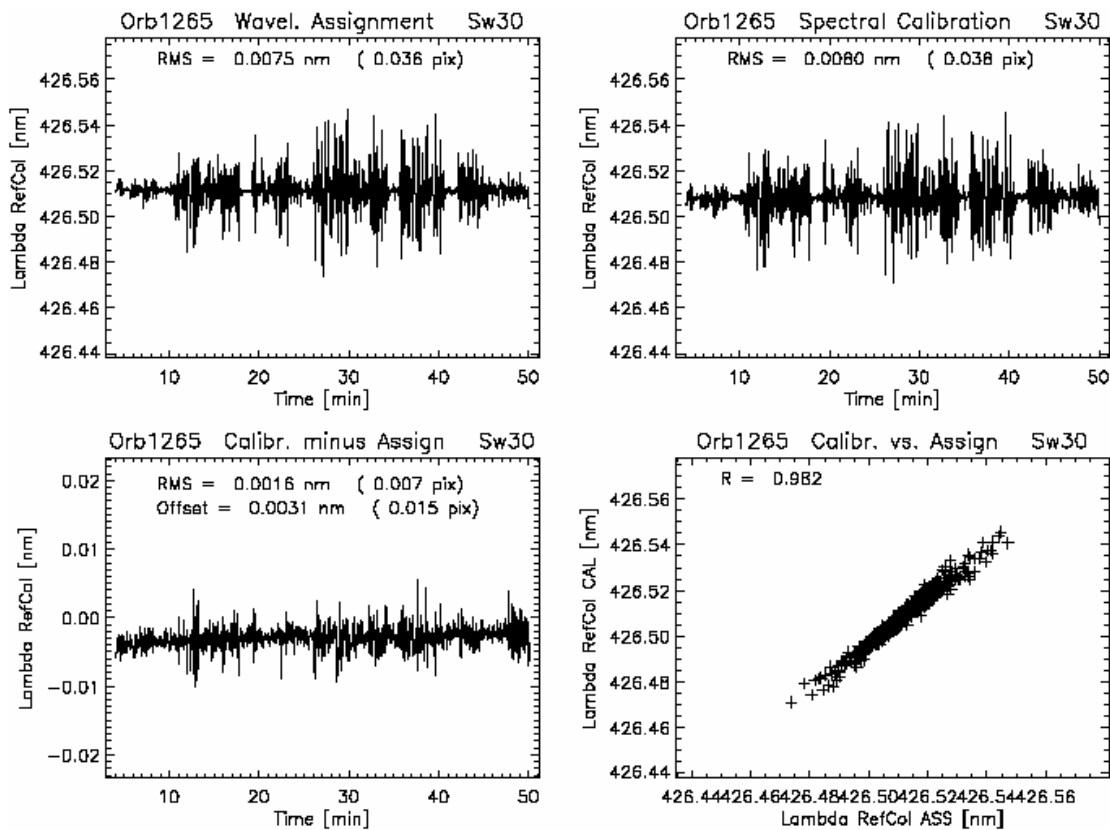


Figure 3 Results from the inhomogeneous slit illumination wavelength correction; top right the observed variability after wavelength calibration of individual spectra; the top left shows the calculated variability from the observed rate of change in the ‘small pixel radiance’ with the high degree of correlation; the bottom right panel shows the correlation coefficient itself and the bottom left panel shows the residual wavelength differences between the spectral calibration result and the corrected wavelengths in the LIB product

The 4-panel image in Figure 3 shows on the top right the observed variability when each individual spectrum is wavelength calibrated. The top left shows the calculated variability when using the observed rate of change in the ‘small pixel radiance’. One immediately sees the high degree of correlation, which is also shown in the bottom right panel, where it can be seen that the correlation coefficient between the two signals is almost 1. The bottom left panel shows the residual wavelength difference between the spectral calibration result and the calculated (assigned) wavelengths in the L1B product. The RMS difference between the two is less than 1/100th of a pixel, which is the requirement on the accuracy of the wavelength scale. Concluding one can say that the effect of the inhomogeneous slit illumination is well understood and corrected for in the science data.

4. Fitting the solar spectrum

Most retrievals of trace gas total columns and profiles fit the earth reflected radiances divided by a solar irradiance measurement. This effectively eliminates the effect of the sun in the radiance spectrum and highlights the effect that the atmosphere has on it, thus facilitating the trace gas retrievals. Furthermore, this method also eliminates most of the instrumental features that are common in both measurements. And since the design of the OMI instrument is such that the light path of the solar and earth reflected measurements are almost identical, this takes care of a lot of possibly not fully explained structure in either spectrum. The main difference between the light paths is that earth reflectance light is reflected off the primary telescope mirror on the entrance slit, whereas solar light enters the OMI via a diffusor (usually the volume diffusor) and is then reflected off a folding mirror into the spectrograph. The effect that this diffusor has on the spectrum has been extensively studied and shown to be less than 0.1 percent of the signal¹.

Fitting the solar spectrum itself is more fraught with difficulties. Any instrumental effect will show up in the spectrum and has to be accounted for. There are many components that influence the final fitting result. In this section we show how we fit the solar spectrum and to what extent we are able to explain all features in the solar measurement. The principle of fitting an OMI solar measurement is straightforward:

1. Take a high-resolution solar reference spectrum
2. Convolve this spectrum with the instrument slit function
3. Spline this to the measurement wavelength scale

The main components that influence the result are: the high resolution solar reference spectrum, the spectral slit function and the wavelength calibration.

The high resolution solar reference spectrum that we use is based on the spectrum that was published by Chance and Spurr⁵ and that has been widely used. The wavelength scale of this spectrum is very accurate (approximately 0.001 nm), but the main drawback is that it contains traces of atmospheric absorption. Therefore we have modified this spectrum by fitting it to lower resolution reference spectra that are much less influenced by atmospheric effects.

In order to simulate the OMI solar measurement we need to have an accurate knowledge of the instrument slit function. This was measured pre-flight with a purpose-built instrument. Consequently the slit function both as a function of wavelength and in the swath direction are known to a high degree of accuracy.

The wavelength calibration is described above. The accuracy of the wavelength scale in the L1B solar product is estimated to be on the order of 1/100th of a pixel, or 0.002 nm.

The current status of our understanding of the solar spectrum as measured by OMI is illustrated in figure 4. We show an OMI solar measurement divided by the simulated OMI spectrum as described above. The absolute radiometric calibration is based on on-ground measurements and appear to be correct within a few percent. In addition there is some residual structure e.g. in the UV-1 and the VIS channels. It is still under investigation whether this is due to imperfections in the radiometric calibration, the slit function, the wavelength calibration of the solar reference spectrum.

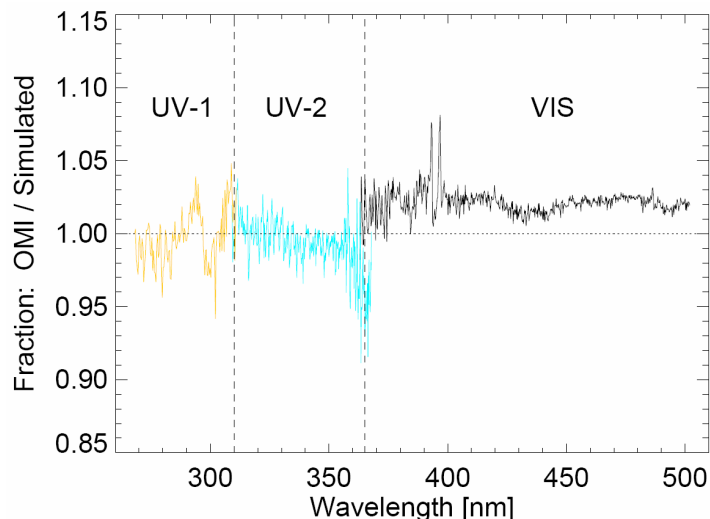


Figure 4 The current status of our understanding of the solar spectrum as measured by OMI as shown by an OMI solar measurement divided by the simulated OMI spectrum as described in the text

5. OMI STRAY LIGHT AND CORRECTION ALGORITHM

5.1 Description of the existing stray light algorithm

The launch version stray light algorithm of OMI is meant to correct for spectral stray light, being stray light generated at the higher OMI wavelengths and causing a spurious contribution at the extreme UV wavelengths of 270 to 290 nm via the extremely high spectral gradient in Earth shine radiance at around 300 - 310 nm. The algorithm has the following main properties.

It computes by the average radiance level seen in a series of wavelength bands (= source contributions) and multiplies this with polynomials to yield a wavelength dependent and swath independent stray light level per sub-channel. The source radiance levels are also averaged over all swath viewing angles.

The computed stray light is applied to entire sub-channels to avoid discontinuities within the sub-channels. The averaging of all swath angles was based on the fact that no significant spatial effect could be seen in the UV1 from nadir port stray light measurements with band passes of 320 and 360 nm, as measured in the calibration period before launch. Although we did expect that the grating would cause part of the stray light in the proper viewing direction, this was happily accepted because an earlier version of the stray light algorithm, without the swath averaging, was computationally quite inefficient.

5.2 Developing a method to analyze in-orbit measurement data

One of the most straightforward means to evaluate in-orbit stray light, is to check for cloud residues at wavelengths where clouds are physically not expected to be observable. Given the wavelength range of OMI, we should observe the radiance at 280 nm, for two reasons.

- Due to ozone absorption, radiance at this wavelength results from scattering high in the atmosphere where clouds are not present
- Within the OMI range the sun spectrum has a minimum at 280 nm, allowing best detection of offset-like effects

The assumption is reasonable for most latitudes, but we have to be aware that close to poles there is a risk of high PSC's physically showing up at 280 nm. This is especially so in ozone hole conditions.

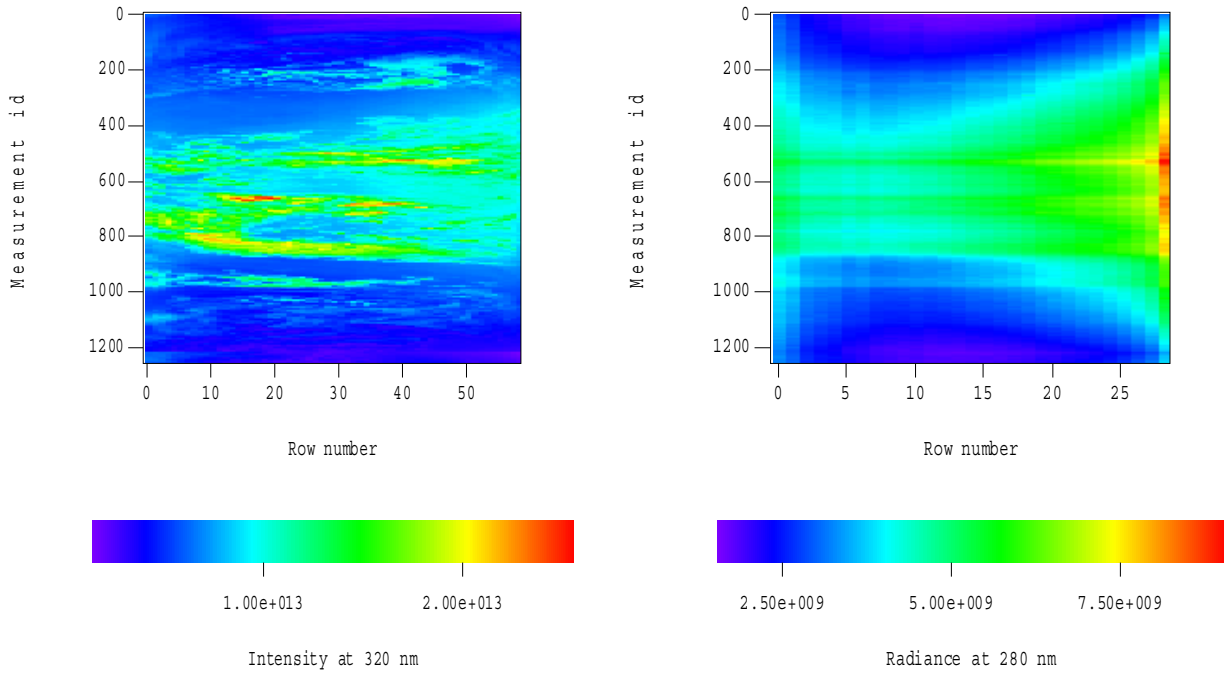


Figure 5 Radiance at 320 nm and at 280 nm as a function of measurement id (~latitude) and detector pixels for the across track swath; the 320 nm graph shows actual clouds and the 280 nm graph cloud residues due to stray light (stray light correction is not applied), together with a sun illumination / scattering effect.

Note that the numeric for the color scale at the bottom of the graphs is linear, for this and all subsequent graphs

Figure 5 shows example graphs of radiance at 320 nm, to show cloud structures, and 280 nm to show residues. the graphs have a measurement id on the vertical axis, which agrees with the latitude for a single orbit and, on the horizontal axis a row number, agreeing with the swath. In Figure 5 the stray light algorithm is not applied, meaning that the residues from stray light are clearly visible and agreeing with the structures from the cloud graph (left).

However, the residues are obscured by the variation of the radiance over the orbit. To remove this effect, we use the offset to a fitted sun spectrum rather than the 280 nm radiance level.

The fit model is as follows.

$$F(\lambda) = P_a(\lambda - \lambda_0).S(\lambda') + P_b(\lambda - \lambda_0) + c_0.Ring(\lambda) \quad (1)$$

Where

- F model to fit the measurement data
- λ wavelength
- λ_0 reference wavelength, taken close to 280 nm
- λ' $=\lambda + F_{shift} + (\lambda-\lambda_0).F_{squeeze}$, via fitting F_{shift} and/or $F_{squeeze}$ effectively a wavelength adjustment mechanism is included to reduce sensitivity to the specific wavelength scale used
- S sun spectrum, convoluted with an OMI slit function
- P_a polynomial sun multiplication factor, $P_a(x)=a_0+a_1.x+a_2.x^2+..$
- P_b offset polynomial, $P_b(x)=b_0+b_1.x+b_2.x^2+..$
- Ring Ring spectrum
- c_0 multiplying factor for the Ring spectrum

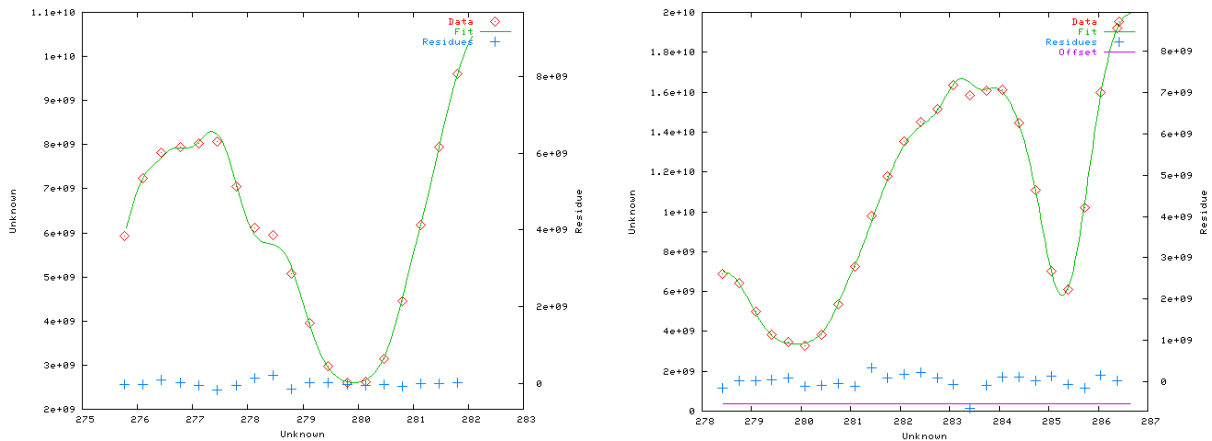


Figure 6 Two fits of a typical Earth measurement at around 280 nm; the data, fit and offset use the left scale and the residues the right; the residues are defined as the difference between data and fit

Figure 6 shows two fits of a typical radiance spectrum and using the model from equation (1). The fits uses a third order sun multiplication polynomial to mimic atmospheric scattering and ozone absorption (a_0 , a_1 , a_2 and a_3 fitted) and a single term offset (only b_0 is fitted). Instead of fitting the Ring spectrum (c_0), we decided to use the lower wavelength range (right graph) because it has less high gradients and in shape almost equals the Ring spectrum. Therefore in this wavelength section, not using the Ring spectrum is expected to have only a limited impact.

Despite the slight mismatches of the fits seen at 287 and at 283 nm, the fit is considered sufficiently good to reveal the offset and thereby the stray light residues. The mismatches exceed the noise and may either be due to an inaccuracy in the reference sun spectrum used or in the slit function.

Figure 7 shows the fitted offset (parameter b_0) and sun intensity factor (parameter a_0) for the same data as in Figure 6, again distributed over an orbit. The graphs were obtained after applying all level 0-1b correction algorithms but without stray light correction. This shows that residues from clouds appear as offset from sun intensity effects and that this offset is fairly free from sun intensity effects.

From Figure 7 we see that the offset clearly is related to clouds effects and can therefore be attributed residual stray light.

5.3 Performance of the existing algorithm

Figure 8 shows the cloud structure and stray light residues after applying the stray light algorithm and using the sun spectrum fit as explained above and as a function of the swath (horizontal axis) and the measurement id (=latitude, vertical axis).

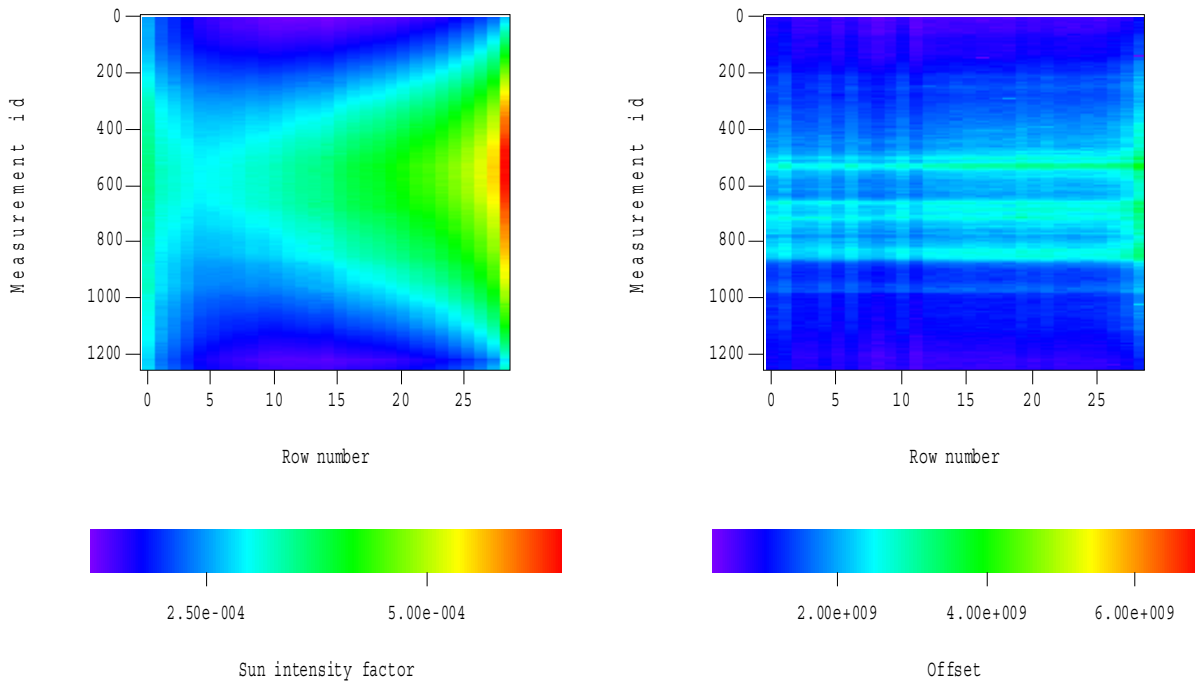


Figure 7 Separation of stray light at 280 nm and sun intensity effects; the left graph shows the fitted sun intensity where the horizontal axis represents the swath perpendicular to the flight direction and the vertical axis the measurement number representing the flight direction or latitude; the right graph shows the fitted sun spectrum offset, representing stray light residues

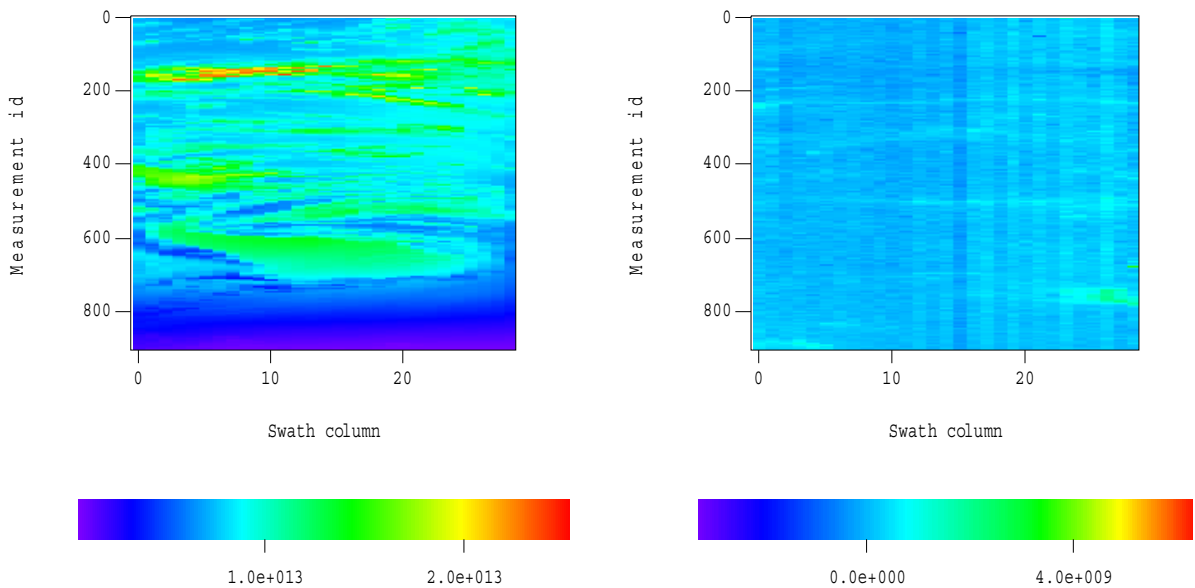


Figure 8 Cloud structure at 320 nm for orbit 4708 (left graph) and the offset residue (right graph), both as a function of the swath (horizontal axis) and the measurement id (=latitude, vertical axis).

Analysing Figures 7 and 8 we have the following conclusions.

- Without stray light correction, there are very clear cloud residues in the 280 nm offset; they are up to 10 % of the useful signal at 270 nm
- With stray light correction, the residues have decreased to maximum about 3 % of the useful signal at 270 nm
- With stray light correction, the more detailed view on the residues (Figures 8 and 9) show they are a function of the swath

5.4 Delta stray light correction

The residues shown above are expected to be related to cloud structures as seen in the wavelengths above about 295 nm. This has been made plausible from the combination of Figures 5 (left graph) and Figure 7 (right graph) and from Figure 8 (comparing the left and right graphs).

Assuming that the relation is correct, we can express the residuals as a linear combination of cloud structures, in the following way.

$$S_{offset}(i) = \sum_j \sum_k a_{i,j,k} \cdot S_{cloud}(j,k) \quad (2)$$

Where

S_{offset}	delta offset, resulting in features if plotted as a function of measurement id or swath
I	counter related to sets of swath pixels in the target area (offset at around 280 nm)
J	counter related to sets of swath pixels in the source area (clouds above 295 nm)
k	counter related to wavelength
$a_{i,j,k}$	correlation coefficient
S_{cloud}	radiance at a wavelength where clouds show up and for a given set of swath pixels

The relation uses sets of swath pixels (counters i and j) instead of single swath pixels to reduce the size of the correlation cube, i.e. with 5 offset swath regions (averaging about 6 pixels in a total of 28 swath pixels), also 5 swath cloud pixels and 12 sampling wavelengths (295, 300, 305, 311, 320, 330, 340, 350, 360, 380, 430 and 460 nm), we end up with $5 \times 5 \times 12 = 300$ parameters. When excluding swath dependency, we have 12 parameters and those parameters represent adjustment factors for the launch version stray light algorithm.

The parameters are obtained via fitting a set of S_{cloud} 's to S_{offset} in larger data sets, complete orbits or the cloudy parts of those. The fits have been performed for various amounts of parameters and did not show any singular values. This indicates that also the cloud distribution at the sampling wavelengths are sufficiently different. For the swath this is evident, for the wavelength this is less evident as different wavelengths observe the same clouds although with a different amount of molecular scattering included.

Figure 9 shows two plots where 5 offset and 5 cloud swath regions were used.

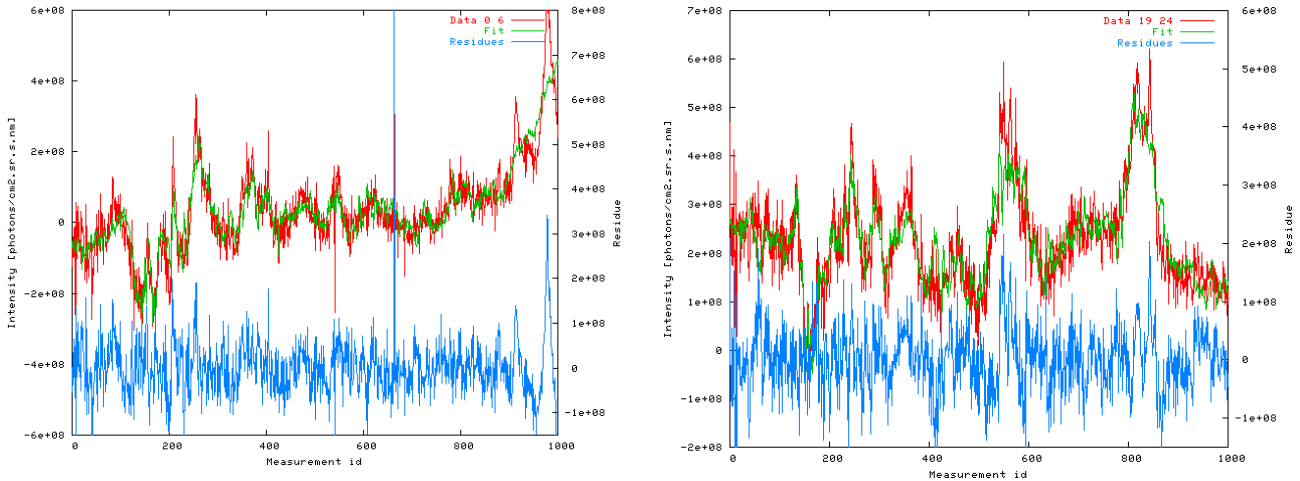


Figure 9 Plots where 5 offset and 5 cloud swath regions were used and 12 wavelength samples; the upper part of the graphs show the offset together with the fit (left axis) and the lower part the residues (right axis); the graphs include both nice matches and lack of fit (especially the left graph, measurement id's 900 to 1000)

It appears that most of the (along-orbit) structures in the offset can be described properly as long as the amount of offset and swath cloud regions is sufficient. The exception are some features at high latitudes which are present in the offset data but not in the cloud data. This may be caused by thin and high PSC's but this has not been thoroughly checked.

Figure 10 shows typical results after applying OMI's launch version stray light correction followed by a delta correction based on equation (2). The Figure shows two typical profiles from the offset image (Figure 8, right graph), before and after applying the delta correction. After correction, the residues sizes are considerably improved and are maximum about 1 % of the useful signal at 270 nm.

However, this is a first test result and before accepting the result the delta algorithm should be tested on larger data sets and the results should be checked for exceptions and their origins.

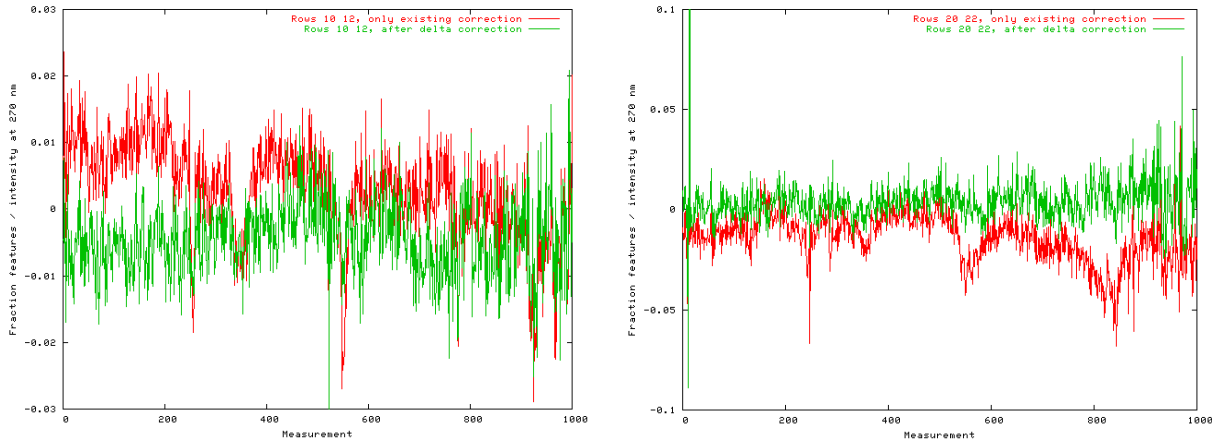


Figure 10 Typical results before and after applying the delta offset correction

6. CONCLUSION

In this paper we have shown that the OMI in-orbit calibration activities are working towards a better understanding of the instrument in orbit. The mechanism of spectral calibration changes resulting from partial filling of the instrument's entrance slit by clouds were discussed and a correction algorithm was described. The current status of the analyses of the solar irradiance measurements has been presented. Spatial structure at wavelengths below 300 nm originating from clouds as observed above 300 nm were presented and discussed. The spectral stray light algorithm has been improved using the available in-flight measurement data. The OMI is already producing the official ozone product for the IPCC.

REFERENCES

1. M. R. Dobber, R. J. Dirksen, P. F. Levelt, G. H. J. van den Oord, R. Voors, Q. Kleipool, G. Jaross, M. Kowalewski, E. Hilsenrath, G. Leppelmeier, J. de Vries, W. Dierssen, N. Rozemeijer "Ozone Monitoring Instrument calibration", IEEE Trans. Geosc. Rem. Sens., accepted for publication.
2. M. Dobber, R. Dirksen, R. Voors, G.H. Mount, P. Levelt, Ground-based zenith sky abundances and in situ gas cross sections for ozone and nitrogen dioxide with the Earth Observing System Aura Ozone Monitoring Instrument, Applied Optics vol. 44, no. 14, 2846-2856.
3. P. F. Levelt, E. Hilsenrath, G. W. Leppelmeier, G. H. J. van den Oord, P. K. Bhartia, J. Tamminen, J. F. de Haan, J. P. Veefkind, "Science objectives of the Ozone Monitoring Instrument", IEEE Trans. Geosc. Rem. Sens., submitted for publication.
4. P. F. Levelt, G. H. J. van den Oord, M. R. Dobber, J. Claas, H. Visser, J. de Vries, "The Ozone Monitoring Instrument", IEEE Trans. Geosc. Rem. Sens., accepted for publication.
5. G. H. J. van den Oord, J. P. Veefkind, P. F. Levelt, M. R. Dobber, "Level 0 to 1B processing and operational aspects", IEEE Trans. Geosc. Rem. Sens., accepted for publication.
6. K. Chance and R.J.D. Spurr, "Ring Effect Studies: Rayleigh scattering, including molecular parameters for Rotational Raman scattering, and the Fraunhofer spectrum", Applied Optics 36, 1997